On multifield inflation, adiabaticity, and the speed of sound of the curvature perturbations

Atal, V.

3

Transient reductions in the speed of sound

In this chapter we will study the observational consequences of a fast evolving speed of sound for the curvature perturbations. This could correspond to inflating in a two-field potential with a sharp turn, as in the left panel of figure 2.4. Transient phenomena during inflation will imply that the predictions for the n-point correlation functions can be modified with respect to the slow-roll predictions shown in Chapter 1. This will demand adopting new techniques both for calculating the observables and for testing the predictions against the CMB data.

First, we apply, compare and extend different techniques for calculating both the power spectrum and bispectrum, based on applying perturbation theory to the Hamiltonian or to the equations of motion. We further check for the possibility that some of the anomalous features found in the Planck data have a common physical origin in a transient reduction of the inflaton speed of sound. We do this by exploiting predicted correlations between the power spectrum and bispectrum. Our results suggest that current data might already be sensitive enough to detect transient reductions in the speed of sound as mild as a few percent. Since this is a signature of interactions, it opens a new window for the detection of extra degrees of freedom during inflation.

This chapter is based on the following two papers:

- *Inflation with moderately sharp features in the speed of sound: Generalized slow roll and in-in formalism for power spectrum and bispectrum*,
  A. Achucarro, V. Atal, B. Hu, P. Ortiz and J. Torrado, Phys. Rev. D **90** (2014) 2, 023511 [arXiv:1404.7522 [astro-ph.CO]].

- *"Localized correlated features in the CMB power spectrum and primordial bispectrum from a transient reduction in the speed of sound,"*,
  A. Achúcarro, V. Atal, P. Ortiz and J. Torrado, Phys. Rev. D **89** (2014) 10, 103006 [arXiv:1311.2552 [astro-ph.CO]].

We have also enlarged the discussion made in these papers in order to contrast our results with the new data analysis of the Planck collaboration.

3.1 Introduction

As we have previously discussed, when an additional heavy field can be consistently integrated out [80, 81, 92, 101–103] (see also [51]), inflation is described by an effective single-field theory [34, 80, 81, 101, 104, 105] with a variable speed of sound. In particular, changes in the speed of sound result from derivative couplings, or equivalently, turns in field space [55, 73, 79, 81, 82, 92, 95, 101, 106]. The effect of a variable speed of sound has been analyzed both in the power spectrum [55, 107, 108] (for sudden variations see [109–113]) and bispectrum [108, 114, 115] (see [112, 113] for sudden variations). Transient variations in the speed of sound will produce *oscillatory* and *correlated* features in the correlation functions of the adiabatic curvature perturbation [34, 108, 109, 111, 113, 116–119]. These effects are worth taking into account since an oscillatory component in the correlation functions may improve the fits in comparison with a flat primordial spectra, and because we expect correlations to be very good model selectors.

Apart from reduction in the speed of sound, several other mechanisms during inflation also produce oscillatory features. As first noted in [44], a step in the inflaton potential causes features in the spectra [47–49, 113, 120–126]. Different initial vacuum states (see e.g. [127–130]) or multi-field dynamics [82, 117, 131, 132] may also cause oscillations in the primordial spectra.

Whether an oscillatory primordial power spectrum is preferred in the data is a question that has been asked by several authors. Searches in the CMB power spectrum data have been performed for a variety of scenarios, such as transient slow-roll violations [110, 124, 133–138], superimposed oscillations in the primordial power spectrum [139–145] and more general parametric forms (see [30] and references therein). In addition, the Planck collaboration searched for features in the CMB bispectrum for a number of theoretically motivated templates [40]. In none of these cases the statistical significance of the extended models has been found high enough to claim a detection. Still, it is becoming clear that hints of new physics (if any) are most likely to be detected in the correlation between different observables.

The detection of transients poses some interesting challenges. In particular, the effects of a feature in the potential or a localized change in the speed of sound depend on its *location* (in time or e-folds), its *amplitude* and its *sharpness* (or inverse duration). If transients are too sharp, they can excite higher frequency modes that make the single-field interpretation inconsistent (as extensively discussed in Chapter 2). Notably, some of the best fits found so far in the data for a step feature in the potential [136, 146, 147] falls outside the weakly coupled regime that is implicitly required for its interpretation as a step in the single field potential [97, 98]. On the other hand, if the features are too broad, their signature usually becomes degenerate with cosmological parameters, making their presence difficult to discern. There is however an interesting intermediate regime where the features are mild (small amplitude) and moderately sharp, which makes them potentially detectable in the CMB/LSS data, while they also remain under good theoretical control. This regime is particularly important if the inflaton field excursion is large and can reveal features in the inflationary potential and the presence of other degrees of freedom. At the same time, if slow-roll is the result of a (mildly broken) symmetry that protects the background in the UV completion, the same symmetry might presumably preclude very sharp transients.

In this chapter we first review and enlarge several methods to calculate correlation functions when there are transient phenomena happening during inflaton. Finally, we perform a search for transient reductions in the speed of sound in the CMB data. We do this by exploiting a very simple correlation between power spectrum and bispectrum noted in [108], valid in the mild and sharp regime defined above.

3.2 Moderately sharp variations in the speed of sound: primordial power spectrum and bispectrum

In order to compare any model with data, it is important to develop fast and accurate techniques to compute the relevant observables of the theory, in this case, correlations functions of the adiabatic curvature perturbation. The calculation of correlation functions is often rather complicated and the use of approximate methods is needed. The study of transients often involves deviations from slow-roll and may be analysed in the generalized slow-roll (GSR) formalism [110, 113, 114, 119, 148–152]. This approach is based on solving the equations of motion iteratively using Green's functions method. This formalism can cope with general situations with both slow-roll and speed of sound

features, but one usually needs to impose extra hierarchies between the different parameters to obtain simple analytic solutions.

A notable exception that is theoretically well understood is a transient, mild, and moderately sharp reduction in the speed of sound. They are better defined as those for which the effects coming from a varying speed of sound are small enough to be treated at linear order, but large enough to dominate over the slow-roll corrections. This carries an implicit assumption of uninterrupted slow-roll[1]. We will show that this regime ensures the validity of the effective single-field theory, even though our analysis is blind to the underlying inflationary model. In this regime, an alternative approach is possible, that makes the correlation between power spectrum and bispectrum manifest [108]. This approach is based on applying perturbation theory at the level of the Hamiltonian for both the power spectrum and bispectrum. The change in the power spectrum is then simply given by the Fourier transform of the reduction in the speed of sound, and the *complete* bispectrum can be calculated to leading order in slow-roll as a function of the power spectrum. Hence we name this approximation Slow-Roll Fourier Transform (SRFT). One of the aims of this chapter is to compare the GSR and SRFT approaches. In order to do this, we develop simple expressions within the GSR approach and the in-in formalism for computing the changes in the power spectrum and bispectrum due to moderately sharp features in the speed of sound. These are new and extend the usual GSR expressions for very sharp features.

Additionally, we compute the bispectrum. We compute it from the cubic action for the curvature perturbation $\mathcal{R}(t, \mathbf{x})$ using an approximation for sharp features as in [113], but including the next order correction and additional operators. We check that the agreement with the SRFT result [108] is excellent. An important point we show is that the contributions to the bispectrum arising from the terms proportional to $(1 - c_s^{-2})$ and s in in the cubic action are of the same order, *independently of the sharpness of the feature*. We also eliminate the small discrepancy found in [113] between their bispectrum and the one obtained with GSR [124] for step features in the scalar potential, due to a missing term in the bispectrum.

Our starting point is the action for the adiabatic curvature perturbation $\mathcal{R}(t, \mathbf{x})$. In the framework of the effective field theory (EFT) of inflation [34], this is directly linked to the effective action for the Goldstone boson of time diffeomorphisms $\pi(t, \mathbf{x})$, via the

[1]Here we mean that $\epsilon, \eta \ll 1$. This is not however a necessary condition for making use of the techniques we are presenting, as they can be generalized to the case in which both the speed of sound and the slow roll parameters are subject to transient changes (and hence $\eta > 1$ is allowed) [91]

linear relation[2] $\mathcal{R} = -H\pi$. Let us focus on a slow-roll regime and write the quadratic and cubic actions for π (as written in Chapter 1):

$$S_2 = \int d^4x\, a^3 M_{\rm Pl}^2 \epsilon H^2 \left\{ \frac{\dot\pi^2}{c_s^2} - \frac{1}{a^2}\left(\nabla\pi\right)^2 \right\} \ , \tag{3.1}$$

$$S_3 = \int d^4x\, a^3 M_{\rm Pl}^2 \epsilon H^2 \left\{ -2Hsc_s^{-2}\pi\dot\pi^2 - \left(1-c_s^{-2}\right)\dot\pi\left[\dot\pi^2 - \frac{1}{a^2}\left(\nabla\pi\right)^2\right] \right\} \ , \tag{3.2}$$

where $\epsilon = -\dot H/H^2$ and we are neglecting higher order slow-roll corrections ($\propto \ddot H$). We recall that s parametrizes changes in the speed of sound, $s \equiv \dot c_s/c_s H$, and for convenience we define a new variable u as

$$u \equiv 1 - c_s^{-2} \ . \tag{3.3}$$

In this section we compare the different approaches to evaluating the power spectrum and bispectrum of the adiabatic curvature perturbation from eqs. (3.1) and (3.2) with a variable speed of sound, and show the excellent agreement between them.

3.2.1 Power spectrum and bispectrum with the Slow-Roll Fourier Transform method

Corrections to the two-point function due to a transient reduction in the speed of sound can be calculated using the in-in formalism [153, 154]. We can do it assuming an uninterrupted slow-roll regime, which, as we showed in the Chapter 2, is perfectly consistent with turns along the inflationary trajectory. In order to calculate the power spectrum, we separate the quadratic action (3.1) in a free part and a small perturbation:

$$S_2 = \int d^4x\, a^3 M_{\rm Pl}^2 \epsilon H^2 \left\{ \dot\pi^2 - \frac{1}{a^2}\left(\nabla\pi\right)^2 \right\} - \int d^4x\, a^3 M_{\rm Pl}^2 \epsilon H^2 \left\{ \dot\pi^2 \left(1-c_s^{-2}\right) \right\} \ , \tag{3.4}$$

Then, using the in-in formalism, the change in the power spectrum due to a small transient reduction in the speed of sound can be calculated to first order in u, and it is found to be [108]

$$\frac{\Delta\mathcal{P}_\mathcal{R}}{\mathcal{P}_{\mathcal{R},0}}(k) = k\int_{-\infty}^{0} d\tau\ u(\tau)\sin\left(2k\tau\right) \ , \tag{3.5}$$

where $k \equiv |\mathbf{k}|$, $\mathcal{P}_{\mathcal{R},0} = H^2/(8\pi^2\epsilon M_{\rm Pl}^2)$ is the featureless power spectrum with $c_s = 1$, and τ is the conformal time. We made the implicit assumption that the speed of sound approaches to one asymptotically, since we are perturbing around that value[3]. Here we see that the change in the power spectrum is simply given by the Fourier transform of

[2] In this work, we do not need to consider non-linear correction terms, since we are in a slow-roll regime. For further details on this, see [37].

[3] At the level of the power spectrum, the generalization to arbitrary initial and final values of the speed of sound $c_{s,0}$ is straightforward, provided they are sufficiently close to each other.

the reduction in the speed of sound. Notice that the result above is independent of the physical origin of such reduction.

For the three-point function, we take the cubic action (3.2), and calculate the bispectrum at first order in u and s, which implies that we must have $|u|_{\max}, |s|_{\max} \ll 1$ [4]. We also disregard the typical slow-roll contributions that one expects for a canonical featureless single-field regime [37]. Therefore, for the terms proportional to u and s to give the dominant contribution to the bispectrum, one must require that u and/or s are much larger than the slow-roll parameters, i.e. $\max(u, s) \gg \mathcal{O}(\epsilon, \eta)$. Let us note that eq. (3.5) can be inverted, so that we might write u (or, equivalently c_s) as a function of $\Delta\mathcal{P}_{\mathcal{R}}/\mathcal{P}_{\mathcal{R},0}$. As the bispectrum is a function of c_s as its derivative, we can write the bispectrum as a function of $\Delta\mathcal{P}_{\mathcal{R}}/\mathcal{P}_{\mathcal{R},0}$. Using again the in-in formalism, one finds [108]:

$$\Delta\ B_{\mathcal{R}}(\mathbf{k}_1, \mathbf{k}_2, \mathbf{k}_3) = \frac{(2\pi)^4 \mathcal{P}_{\mathcal{R},0}^2}{(k_1 k_2 k_3)^2} \left\{ -\frac{3}{2}\frac{k_1 k_2}{k_3} \left[\frac{1}{2k}\left(1 + \frac{k_3}{2k}\right)\frac{\Delta\mathcal{P}_{\mathcal{R}}}{\mathcal{P}_{\mathcal{R},0}} - \frac{k_3}{4k^2}\frac{d}{d\log k}\left(\frac{\Delta\mathcal{P}_{\mathcal{R}}}{\mathcal{P}_{\mathcal{R},0}}\right)\right] \right.$$

$$+2 \text{ perm} + \frac{1}{4}\frac{k_1^2 + k_2^2 + k_3^2}{k_1 k_2 k_3}\left[\frac{1}{2k}\left(4k^2 - k_1 k_2 - k_2 k_3 - k_3 k_1 - \frac{k_1 k_2 k_3}{2k}\right)\frac{\Delta\mathcal{P}_{\mathcal{R}}}{\mathcal{P}_{\mathcal{R},0}}\right.$$

$$\left.\left. - \frac{k_1 k_2 + k_2 k_3 + k_3 k_1}{2k}\frac{d}{d\log k}\left(\frac{\Delta\mathcal{P}_{\mathcal{R}}}{\mathcal{P}_{\mathcal{R},0}}\right) + \frac{k_1 k_2 k_3}{4k^2}\frac{d^2}{d\log k^2}\left(\frac{\Delta\mathcal{P}_{\mathcal{R}}}{\mathcal{P}_{\mathcal{R},0}}\right)\right]\right\}\Bigg|_{k=\frac{1}{2}\sum_i k_i}, \quad (3.6)$$

where $k_i \equiv |\mathbf{k}_i|$, $k \equiv (k_1 + k_2 + k_3)/2$, and $\Delta\mathcal{P}_{\mathcal{R}}/\mathcal{P}_{\mathcal{R},0}$ and its derivatives are evaluated at k. From the result above it is clear how features in the power spectrum seed correlated features in the bispectrum. Note that in the squeezed limit ($k_1 \to 0, k_2 = k_3 = k$) one recovers the single-field consistency relation [37, 155].

In the following sections, we compute the power spectrum and bispectrum using alternative methods and compare the results.

3.2.2 Power spectrum in the GSR formalism

Instead of applying perturbation theory at the level of the Hamiltonian (as we do in the in-in formalism), one can calculate the power spectrum by solving iteratively the full equations of motion (first in [148, 149] and further developed in [107, 114, 119, 124, 150, 151]). The idea is to consider the Mukhanov-Sasaki equation of motion with a

[4] This is a conservative choice, values of $s > 1$ might be consistent with perturbativity, as discussed in Chapter 2

time-dependent speed of sound. We recall it from eq. (1.41), namely:

$$\frac{d^2 v_{\mathbf{k}}(\tau)}{d\tau^2} + \left(c_s^2 k^2 - \frac{1}{z}\frac{d^2 z}{d\tau^2} \right) v_{\mathbf{k}}(\tau) = 0 \ , \tag{3.7}$$

with $v = z\mathcal{R}$, $z^2 = 2a^2 \epsilon c_s^{-2}$ and

$$\frac{1}{z}\frac{d^2 z}{d\tau^2} = a^2 H^2 \Big[2 + 2\epsilon - 3\tilde{\eta} - 3s + 2\epsilon(\epsilon - 2\tilde{\eta} - s) + s(2\tilde{\eta} + 2s - t) + \tilde{\eta}\tilde{\xi} \Big] \ , \tag{3.8}$$

where we have used the following relations:

$$\epsilon = -\frac{\dot{H}}{H^2} \quad , \quad \tilde{\eta} = \epsilon - \frac{\dot{\epsilon}}{2H\epsilon} \quad , \quad s = \frac{\dot{c}_s}{H c_s} \quad , \quad t = \frac{\ddot{c}_s}{H\dot{c}_s} \quad , \quad \tilde{\xi} = \epsilon + \tilde{\eta} - \frac{\dot{\tilde{\eta}}}{H\tilde{\eta}} \ , \tag{3.9}$$

and here the dot denotes the derivative with respect to cosmic time. Defining a new time variable $d\tau_c = c_s d\tau$ and a rescaled field $y = \sqrt{2kc_s}v$, the above equation can be written in the form:

$$\frac{d^2 y}{d\tau_c^2} + \left(k^2 - \frac{2}{\tau_c^2} \right) y = \frac{g\,(\ln \tau_c)}{\tau_c^2} y \ , \tag{3.10}$$

where

$$g \equiv \frac{f'' - 3f'}{f} \qquad , \quad f = 2\pi z c_s^{1/2} \tau_c \ , \tag{3.11}$$

and $'$ denotes derivatives with respect to $\ln \tau_c$. Throughout this section (and only in this section), unless explicitly indicated, we will adopt the convention of positive conformal time ($\tau, \tau_c \geq 0$) in order to facilitate comparison with [107, 151]. Note that g encodes all the information with respect to features in the background. In this sense, setting g to zero represents solving the equation of motion for a perfect de Sitter universe, where the solution to the mode function is well known. Considering the r.h.s. of equation (3.10) as an external source, a solution to the mode function can be written in terms of the homogeneous solution. In doing so, we need to expand the mode function in the r.h.s. as the homogeneous solution plus deviations and then solve iteratively. To first order, the contribution to the power spectrum is of the form [151]:

$$\ln \mathcal{P}_{\mathcal{R}} = \ln \mathcal{P}_{\mathcal{R},0} + \int_{-\infty}^{\infty} d \ln \tau_c \, W\,(k\tau_c)\, G'\,(\tau_c) \, , \tag{3.12}$$

where the logarithmic derivative of the source function G reads:

$$G' = -2(\ln f)' + \frac{2}{3}(\ln f)'' \ , \tag{3.13}$$

and the window function W and its logarithmic derivative (used below) are given by

$$W(x) = \frac{3\sin(2x)}{2x^3} - \frac{3\cos(2x)}{x^2} - \frac{3\sin(2x)}{2x} \ , \tag{3.14}$$

$$W'(x) \equiv \frac{dW(x)}{d\ln x} = \left(-3 + \frac{9}{x^2}\right)\cos(2x) + \left(\frac{15}{2x} - \frac{9}{2x^3}\right)\sin(2x) \ . \tag{3.15}$$

If we consider moderately sharp features in the speed of sound, such that $\epsilon, \tilde{\eta} \ll s, t$, the leading contribution to the function G' is the following:

$$G' = -\frac{2}{3}s + \frac{2}{3}\left(\frac{aH\tau_c}{c_s} - 1\right)^2 + \frac{2}{3}\left(\frac{aH\tau_c}{c_s} - 1\right)(4 - s) + \frac{1}{3}\left(\frac{aH\tau_c}{c_s}\right)^2 s\,(-3 + 2s - t) \ , \tag{3.16}$$

where t is defined in (3.9). Moreover, when $|s| \ll 1$ but $t \gtrsim \mathcal{O}(1)$, the logarithmic derivative of G is approximately given by:

$$G' \simeq s - \frac{\dot{s}}{3H} \ , \tag{3.17}$$

where we have used that $aH\tau_c/c_s \simeq 1 + s$. This result agrees with the results of [107] in the mentioned limits. In this approximation, the leading contribution to the power spectrum is:

$$\ln \mathcal{P}_{\mathcal{R}} \simeq \ln \mathcal{P}_{\mathcal{R},0} + \int_{-\infty}^{\infty} d\ln\tau_c \left[W(k\tau_c)s\,(\tau_c) - \frac{1}{3}W\,(k\tau_c)\,\frac{ds}{d\ln\tau_c}\right] \ . \tag{3.18}$$

Integrating by parts the term proportional to the derivative of s we obtain:

$$\begin{aligned} \ln \mathcal{P}_{\mathcal{R}} &\simeq \ln \mathcal{P}_{\mathcal{R},0} + \int_{-\infty}^{\infty} d\,\ln\tau_c \left[W\,(k\tau_c) + \frac{1}{3}W'\,(k\tau_c)\right] s\,(\tau_c) \\ &= \ln \mathcal{P}_{\mathcal{R},0} + \int_{-\infty}^{\infty} d\,\ln\tau_c \left[\frac{\sin(2k\tau_c)}{k\tau_c} - \cos(2k\tau_c)\right] s\,(\tau_c) \ . \end{aligned} \tag{3.19}$$

This is the result that we will later on compare with the SRFT result given in equation (3.5). Let us recall that the regime in which this expression has been derived is for moderately sharp reductions such that $\mathcal{O}(\epsilon, \eta) \ll s \ll 1$ and $t \gtrsim \mathcal{O}(1)$. We would like to point out that the s term in the source function (3.17) provides the dominant contribution to the power spectrum on large scales. This can be seen by comparing W and W' in eqs. (3.19), which carry the contribution of s and $\dot{s}$, respectively. We will later show that when including this term, the power spectrum at large scales matches the numerical solution considerably better (see figure 3.3).

In the following, we will: **(i)** derive an analytic expression for the power spectrum as in (3.19) solely in terms of c_s in order to connect with the SRFT approach. **(ii)** Find

an analytic approximation for arbitrary functional forms of the speed of sound in the moderately sharp regime specified above.

(i) For the first point, one can integrate by parts (3.19) in order to get a formula than only involves the speed of sound. Doing so, we obtain:

$$\ln \mathcal{P}_{\mathcal{R}} = \ln \mathcal{P}_{\mathcal{R},0} - \int_{-\infty}^{\infty} d\, \ln \tau_c \left[2\cos(2k\tau_c) - \frac{\sin(2k\tau_c)}{k\tau_c} + 2k\tau_c \sin(2k\tau_c) \right] \ln c_s\left(\tau_c\right) \ , \tag{3.20}$$

where we have used that $s \simeq d\ln c_s / d\ln \tau_c$ and that the asymptotic value of the speed of sound is one, otherwise the boundary term would not vanish. Therefore, the expression above is only valid for functional forms of the speed of sound that satisfy $c_s(\tau = 0) = c_s(\tau = \infty) = 1$. Let us restrict our attention to mild reductions of the speed of sound $|u| = |1 - c_s^{-2}| \ll 1$, in which the SRFT approach is operative. In that case, for mild and moderately sharp reductions, the time τ_c is very well approximated by $\tau_c \simeq \tau$. Furthermore, the logarithmic term of the speed of sound can be expanded as follows:

$$\ln c_s(\tau) \simeq \frac{1}{2}\left(1 - c_s^{-2}(\tau)\right) + \mathcal{O}(u^2) \ . \tag{3.21}$$

Using the expansion above and the fact that $\ln(\mathcal{P}_{\mathcal{R}}/\mathcal{P}_{\mathcal{R},0}) = \ln(1 + \Delta\mathcal{P}_{\mathcal{R}}/\mathcal{P}_{\mathcal{R},0}) \simeq \Delta\mathcal{P}_{\mathcal{R}}/\mathcal{P}_{\mathcal{R},0}$, we can write:

$$\frac{\Delta\mathcal{P}_{\mathcal{R}}}{\mathcal{P}_{\mathcal{R},0}} \simeq k\int_{-\infty}^{0} d\tau\, \left(1 - c_s^{-2}\right) \left[\sin(2k\tau) + \frac{1}{k\tau}\cos(2k\tau) - \frac{1}{2k^2\tau^2}\sin(2k\tau) \right] \tag{3.22}$$

$$\simeq \begin{cases} \left.\frac{\Delta\mathcal{P}_{\mathcal{R}}}{\mathcal{P}_{\mathcal{R},0}}\right|_{\text{SRFT}} + \mathcal{O}\left[(k\tau)^2\right] \ , \ k\tau \ll 1 \\ \\ \left.\frac{\Delta\mathcal{P}_{\mathcal{R}}}{\mathcal{P}_{\mathcal{R},0}}\right|_{\text{SRFT}} + \mathcal{O}\left[(k\tau)^{-1}\right] \ , \ k\tau \gg 1 \end{cases}$$

where we have already returned to negative conformal time. Notice that when $k\tau \ll 1$ we retrieve the SRFT expression (3.5) with a subleading correction $\mathcal{O}(k\tau)$ inside the integral, and that for $k\tau \gg 1$ we also retrieve the SRFT result. The regime $k\tau \sim 1$ will generally involve large scales, where the change in the power spectrum is small, as can be seen in figure 3.3.

(ii) In what follows we derive an analytic approximation to the power spectrum (3.19) for *generic* forms of the speed of sound, provided they are moderately sharp, i.e. $\mathcal{O}(\epsilon, \eta) \ll s \ll 1$ and $t \gtrsim \mathcal{O}(1)$. As in **(i)**, in this regime we can safely consider $\tau_c \simeq c_{s,0}\tau$. Let us drop the rest of assumptions made in point **(i)**, which were only made to establish connection with the SRFT approach. We define the function $X(k\tau_c) \equiv -W'(k\tau_c) -$

$3W(k\tau_c)$, which in general can be decomposed as follows:

$$X(kc_{s,0}\tau) = p_c(kc_{s,0}\tau)\cos(2kc_{s,0}\tau) + p_s(kc_{s,0}\tau)\sin(2kc_{s,0}\tau) \ , \tag{3.23}$$

where p_c and p_s denote the polynomials multiplying the cosine and sine, respectively. Following [113], we will parametrize c_s^2 in terms of the height σ_* and the sharpness β_s of the feature, and a function F describing the shape of the variation of the speed of sound:

$$c_s^2(\tau) = c_{s,0}^2\left[1 - \sigma_* F\left(-\beta_s \ln\tfrac{\tau}{\tau_f}\right)\right] \ , \tag{3.24}$$

where τ_f is the characteristic time of the feature and we take $\sigma_* \ll 1$ to focus on small variations. The rate of change in the speed of sound can be written at first order in σ_* as follows:

$$s(\tau) = -\frac{1}{2}\sigma_*\beta_s F'\left(-\beta_s \ln\tfrac{\tau}{\tau_f}\right) + \mathcal{O}\left(\sigma_*^2\right) \ , \tag{3.25}$$

where $'$ denotes the derivative with respect to the argument. Since we are considering sharp features happening around the time τ_f, the functions involved in the integral of equation (3.19) will only contribute for values in the neighborhood of τ_f. Note that for polynomials with negative powers of $k\tau$, the approximation of evaluating them at $k\tau_f$ fails for small values of $k\tau$, since in that region they vary very rapidly. This may cause infrared divergences in the spectrum which, as we will see, can be cured by approximating the polynomials to first order around $k\tau_f$.

First, we define the variable $y \equiv -\beta_s \ln(\tau/\tau_f)$, and we expand the functions around $\tau = \tau_f$, which is equivalent to $y/\beta_s \ll 1$. Then, at first order, the expansion of X in (3.23) reads:

$$\begin{aligned} X(kc_{s,0}\tau) \simeq & \left[p_c\left(kc_{s,0}\tau_f\right) - y\frac{k\tau_f}{\beta_s}\frac{dp_c}{d(k\tau)}\bigg|_{\tau_f}\right]\cos\left[2kc_{s,0}\tau_f\left(1-\tfrac{y}{\beta_s}\right)\right] \\ & + \left[p_s\left(kc_{s,0}\tau_f\right) - y\frac{k\tau_f}{\beta_s}\frac{dp_s}{d(k\tau)}\bigg|_{\tau_f}\right]\sin\left[2kc_{s,0}\tau_f\left(1-\tfrac{y}{\beta_s}\right)\right] \ . \end{aligned} \tag{3.26}$$

Substituting in (3.19) the above expansion and the definition of s (3.25), the change in the power spectrum is given by:

$$\frac{\Delta\mathcal{P}_{\mathcal{R}}}{\mathcal{P}_{\mathcal{R},0}} = \frac{\sigma_*}{6}\left\{\Big[p_c\cos\left(2kc_{s,0}\tau_f\right)+p_s\sin\left(2kc_{s,0}\tau_f\right)\Big]\int_{-\infty}^{\infty}dy\,\cos\left(\frac{2kc_{s,0}\tau_f}{\beta_s}y\right)F'\left(y\right)\right.$$

$$+\Big[p_c\sin\left(2kc_{s,0}\tau_f\right)-p_s\cos\left(2kc_{s,0}\tau_f\right)\Big]\int_{-\infty}^{\infty}dy\,\sin\left(\frac{2kc_{s,0}\tau_f}{\beta_s}y\right)F'\left(y\right)$$

$$-\frac{k\tau_f}{\beta_s}\left[\left.\frac{dp_s}{d(k\tau)}\right|_{\tau_f}\sin\left(2kc_{s,0}\tau_f\right)+\left.\frac{dp_c}{d(k\tau)}\right|_{\tau_f}\cos\left(2kc_{s,0}\tau_f\right)\right]\int_{-\infty}^{\infty}dy\,\cos\left(\frac{2kc_{s,0}\tau_f}{\beta_s}y\right)y\,F'\left(y\right)$$

$$\left.+\frac{k\tau_f}{\beta_s}\left[\left.\frac{dp_s}{d(k\tau)}\right|_{\tau_f}\cos\left(2kc_{s,0}\tau_f\right)-\left.\frac{dp_c}{d(k\tau)}\right|_{\tau_f}\sin\left(2kc_{s,0}\tau_f\right)\right]\int_{-\infty}^{\infty}dy\;\;sin\left(\frac{2kc_{s,0}\tau_f}{\beta_s}y\right)y\,F'\left(y\right)\right\}\;.$$

Note that the integrals above are the Fourier transforms of the symmetric and antisymmetric parts of the derivative of the shape function $F = F(y)$. We define the envelope functions resulting from these integrals as follows:

$$\int dy\,\cos\left(\frac{2kc_{s,0}\tau_f}{\beta_s}y\right)F'\equiv\frac{1}{2}\mathcal{D}_A,\quad\int dy\,y\,F'\cos\left(\frac{2kc_{s,0}\tau_f}{\beta_s}y\right)=\frac{\beta_s}{4c_{s,0}\tau_f}\frac{d}{dk}\mathcal{D}_S \qquad (3.27)$$

$$\int dy\,\sin\left(\frac{2kc_{s,0}\tau_f}{\beta_s}y\right)F'\equiv\frac{1}{2}\mathcal{D}_S,\quad\int dy\,y\,F'\sin\left(\frac{2kc_{s,0}\tau_f}{\beta_s}y\right)=-\frac{\beta_s}{4c_{s,0}\tau_f}\frac{d}{dk}\mathcal{D}_A\;, \qquad (3.28)$$

where $\mathcal{D}_S$ and $\mathcal{D}_A$ are the envelope functions corresponding to the symmetric and antisymmetric parts of F, respectively. Finally, the change in the power spectrum can be written as:

$$\frac{\Delta\mathcal{P}_{\mathcal{R}}}{\mathcal{P}_{\mathcal{R},0}} = \frac{\sigma_*}{12}\left\{\Big[p_c\cos\left(2kc_{s,0}\tau_f\right)+p_s\sin\left(2kc_{s,0}\tau_f\right)\Big]\mathcal{D}_A+\Big[p_c\sin\left(2kc_{s,0}\tau_f\right)-p_s\cos\left(2kc_{s,0}\tau_f\right)\Big]\mathcal{D}_S\right\}$$

$$-\frac{\sigma_*}{24c_{s,0}}\left\{\left[\left.\frac{dp_s}{d(k\tau)}\right|_{\tau_f}\sin\left(2kc_{s,0}\tau_f\right)+\left.\frac{dp_c}{d(k\tau)}\right|_{\tau_f}\cos\left(2kc_{s,0}\tau_f\right)\right]k\frac{d}{dk}\mathcal{D}_S\right.$$

$$\left.+\left[\left.\frac{dp_s}{d(k\tau)}\right|_{\tau_f}\cos\left(2kc_{s,0}\tau_f\right)-\left.\frac{dp_c}{d(k\tau)}\right|_{\tau_f}\sin\left(2kc_{s,0}\tau_f\right)\right]k\frac{d}{dk}\mathcal{D}_A\right\} \qquad (3.29)$$

Let us stress that the contributions from the second and third lines are comparable to the ones in the first line. The infrared limit of the symmetric part is finite and tends to zero, which would not have been the case if we had only considered the zeroth order terms (first line). We will now substitute the values of the polynomials for the particular regime we are analyzing, $p_c = 1/3$ and $p_s = -1/(3kc_{s,0}\tau)$. In this case, the change in

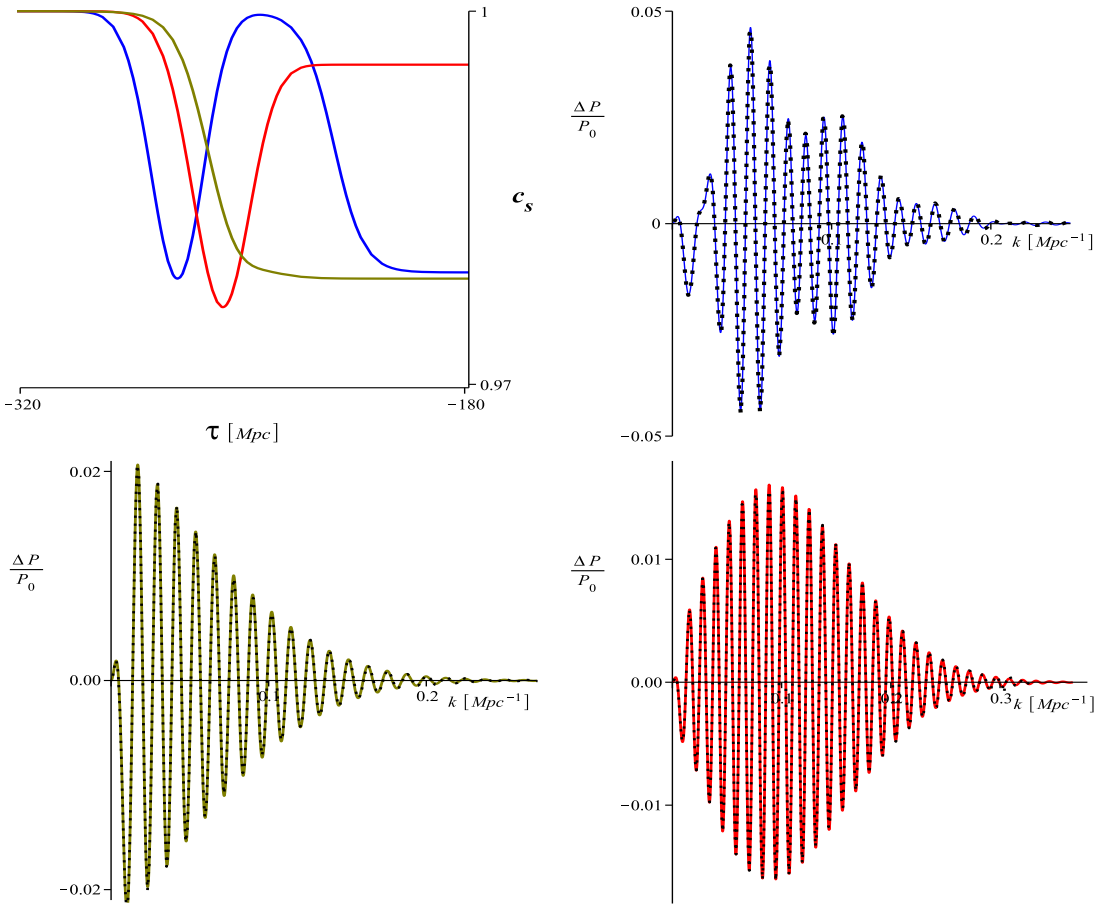

FIGURE 3.1: Speed of sound as defined in (3.31) for three different values of the parameters. We show the power spectra calculated with the full integral (3.19) (dotted line) and with the approximation (3.29) (solid line). The parameters, for the blue, olive and red figures, are respectively given by: $A = [-0.021, -0.0215, -0.0043]$, $B = [-0.043, -0.0086, -0.043]$, $\alpha^2 = [\exp(6.3), \exp(6.3), \exp(7)]$, $\beta_s^2 = [\exp(6.3), \exp(6.3), \exp(7)]$, $\tau_{0_g} = [-\exp(5.6), -\exp(5.55), -\exp(5.55)]$, $\tau_{0_t} = [-\exp(5.4), -\exp(5.55), -\exp(5.55)]$. For the first set of parameters the symmetric and antisymmetric parts have comparable magnitude, while for the second (third) set of parameters the antisymmetric (symmetric) part dominates. As can be seen by the very good agreement between the full integral and the approximation, the chosen parameters are all of them in the sharp feature regime.

the power spectrum reads:

$$\frac{\Delta\mathcal{P}_{\mathcal{R}}}{\mathcal{P}_{\mathcal{R},0}} = \frac{\sigma_*}{36}\left\{\left[\cos\left(2kc_{s,0}\tau_f\right) - \frac{\sin\left(2kc_{s,0}\tau_f\right)}{kc_{s,0}\tau_f}\right]\mathcal{D}_A + \left[\sin\left(2kc_{s,0}\tau_f\right) + \frac{\cos\left(2kc_{s,0}\tau_f\right)}{kc_{s,0}\tau_f}\right]\mathcal{D}_S\right\}$$

$$-\frac{\sigma_*}{72}\left\{\left[\frac{\sin\left(2kc_{s,0}\tau_f\right)}{\left(kc_{s,0}\tau_f\right)^2}\right]k\frac{d}{dk}\mathcal{D}_S + \left[\frac{\cos\left(2kc_{s,0}\tau_f\right)}{\left(kc_{s,0}\tau_f\right)^2}\right]k\frac{d}{dk}\mathcal{D}_A\right\}. \tag{3.30}$$

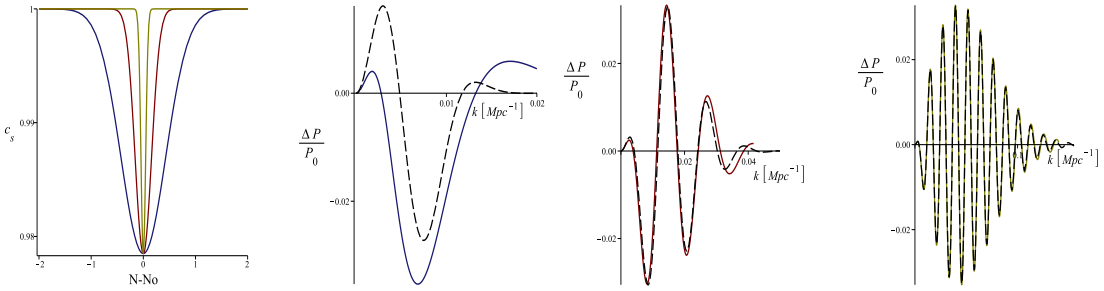

FIGURE 3.2: Here we test when the approximation (3.29) starts to break down. The full integral (3.19) is represented by dashed lines while the approximation (3.29) is given by solid lines. We take $A = 0$, $B = -0.043$, $\tau_{0_g} = -\exp(5.55)$ for the three profiles of the speed of sound, and $\beta_g = [\exp(1), \exp(3), \exp(11/2)]$ for the blue, red and olive figures respectively. We see that the approximation starts to fail for features with $\Delta N \gtrsim 1$.

3.2.2.1 Test for generic variations in the speed of sound

In this section we will test the sharp feature approximation (3.29) in comparison with the full integral (3.19). We explicitly decompose c_s^2 into its symmetric and antisymmetric parts. We choose the following functional form for c_s

$$c_s^2 = 1 + A\left[1 - \tanh\left(\alpha \ln \frac{\tau}{\tau_{0_t}}\right)\right] + B\exp\left[-\beta_s^2\left(\ln\frac{\tau}{\tau_{0_g}}\right)^2\right]$$

$$= \left\{1 + A + B\exp\left[-\beta_s^2\left(\ln\frac{\tau}{\tau_{0_g}}\right)^2\right]\right\}_S + \left\{-A\tanh\left(\alpha\ln\frac{\tau}{\tau_{0_t}}\right)\right\}_A . \qquad (3.31)$$

From the definitions given in eqs. (3.24) and (3.27), the envelope functions are given by

$$\mathcal{D}_A = -\frac{4\pi A}{\sigma_*}\frac{k\tau_{0_t}}{\alpha}\frac{1}{\sinh(\pi k\tau_{0_t}/\alpha)} \quad , \quad \mathcal{D}_S = \frac{4\sqrt{\pi}B}{\sigma_*}\frac{k\tau_{0_g}}{\beta_s}\exp\left(-\frac{k^2\tau_{0_g}^2}{\beta_s^2}\right) . \qquad (3.32)$$

Since the symmetric and antisymmetric parts do not necessarily peak at the same time, the integrands involved in each part take values around τ_{0_g} and τ_{0_t}, respectively. We test our approximation for different values of the parameters above, and show our results in figure 3.1. We can see that the approximation is indeed very good, and that it allows to reproduce highly non-trivial power spectra. By allowing β_s and/or α to be small, we can see where the approximation starts to fail. We show these results in figure 3.2, where one can see that for features with $\Delta N \gtrsim 1$ the approximation breaks down.

3.2.3 Comparison of power spectra

In this section we apply both SRFT and GSR methods for moderately sharp reductions to calculate the change in the power spectrum, and compare them with the power

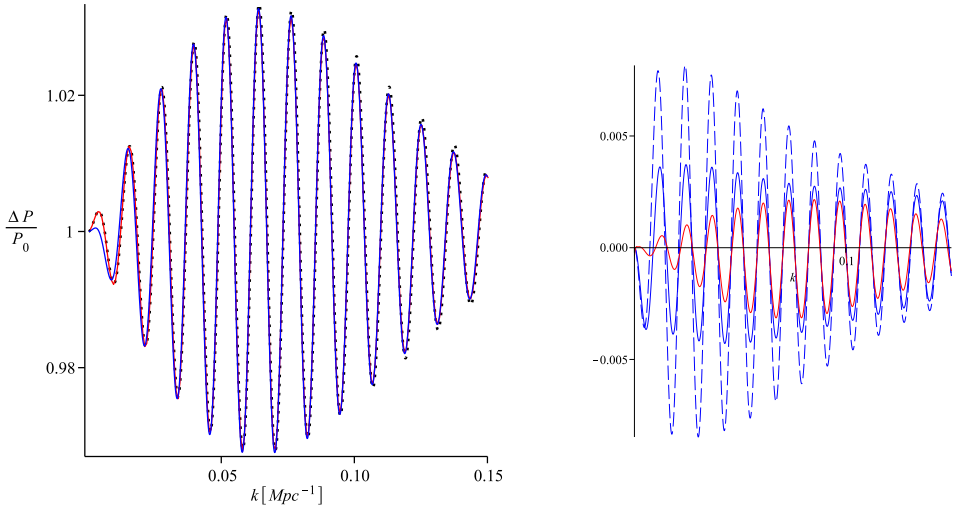

FIGURE 3.3: Change in the power spectrum due to a reduced speed of sound given by (3.33), with the following choice of parameters: $B = -0.043$, $\beta_s = 23.34$, $\ln(\tau_f) = 5.55$, corresponding to one of our best fits to the Planck CMB power spectrum [156]. LEFT: different methods to compute the primordial power spectrum: GSR in the sharp feature approach (blue), SRFT (red), and a solution obtained from the numerical solution to the mode equation (3.7) (black dotted). RIGHT: differences of the GSR sharp feature method (solid blue) and SRFT (red) against the numerical solution. The dashed blue line is the GSR sharp feature approach if we had not taken into account the term proportional to s in the source function (3.17). The numerical solution is calculated choosing $\epsilon \simeq 1.25 \times 10^{-4}$ and $\tilde{\eta} \simeq -0.02$. Higher values of ϵ need a proper accounting for the slow-roll corrections.

spectrum calculated from the numerical solution to the mode equation (3.7). We will test a reduction in the speed of sound purely symmetric in the variable $y = -\beta_s \ln(\tau/\tau_f)$:

$$u = 1 - c_s^{-2} = B\, e^{-\beta_s^2 (N - N_f)^2} = B\, e^{-\beta_s^2 \left(\ln \frac{\tau}{\tau_f}\right)^2} \,. \tag{3.33}$$

In figure 3.3 we show the comparison between the power spectrum coming from the GSR result (3.29) with the one coming form the SRFT method (3.5), and with a numerical solution. In general terms, both methods are in good agreement with the numerical solution. We also note that at large scales the SRFT method reproduces the numerical results better than the GSR method. This is partly due to the fact that in the GSR approximation we have only taken a subset of the terms in the source function. The agreement would have been much worse if we had not taken into account the term proportional to s, as the dashed line in the right plot of figure 3.3 indicates. Note that $k\tau_f \sim 1$ corresponds to the first peak in the left plot of figure 3.3, precisely the regime where we expect a discrepancy, as anticipated in eq. (3.23).

This shows that, in the regime of moderately sharp variations of the speed of sound, the simple SRFT formula (3.5) is capable of reproducing the effect of *all* the terms in the equation of motion, and that there is no need to impose any further hierarchy between

the different terms of the equation of motion in order to have a simple expression, as long as slow-roll is uninterrupted.

3.2.4 Bispectrum for moderately sharp reductions

In this section we will compute the change in the bispectrum due to moderately sharp reductions in the speed of sound using the in-in formalism. Instead of the SRFT method reviewed in section 3.2.1, we will compute the bispectrum using an approximation based on sharp features [113], as for the power spectrum. Our starting point is the cubic action in the effective field theory of inflation, where we will only take into account the contribution from variations in the speed of sound at first order:

$$S_3 = \int d^4x\, a^3 M_{\rm Pl}^2 \frac{\epsilon}{H}\left\{2Hsc_s^{-2}\mathcal{R}\dot{\mathcal{R}}^2 + \left(1-c_s^{-2}\right)\dot{\mathcal{R}}\left[\dot{\mathcal{R}}^2 - \frac{1}{a^2}\left(\nabla\mathcal{R}\right)^2\right]\right\}\,, \tag{3.34}$$

with $\mathcal{R} = -\pi H$. For sharp features ($\beta_s \gg 1$) and given the parametrization in (3.24) and (3.25), one is tempted to think that the contribution of s will dominate over the contribution of $(1-c_s^{-2})$. However, we will show that the contributions arising from both terms are of the same order, *independently of the sharpness* β_s. As dictated by the in-in formalism, the three-point correlation function reads:

$$\langle \mathcal{R}_{\mathbf{k}_1}\mathcal{R}_{\mathbf{k}_2}\mathcal{R}_{\mathbf{k}_3}\rangle = \Bigg\langle \mathrm{Re}\left\{2i\,\mathcal{R}_{\mathbf{k}_1}(0)\mathcal{R}_{\mathbf{k}_2}(0)\mathcal{R}_{\mathbf{k}_3}(0)\int_{-\infty}^{0}d\tau\int d^3x\, a^4 M_{\rm Pl}^2\frac{\epsilon}{H}\Big[2Hsc_s^{-2}\mathcal{R}\dot{\mathcal{R}}^2$$

$$+\left(1-c_s^{-2}\right)\dot{\mathcal{R}}^3 - H^2\tau^2\left(1-c_s^{-2}\right)\dot{\mathcal{R}}(\nabla\mathcal{R})^2\Big]\right\}\Bigg\rangle$$

Expressing the functions $\mathcal{R}(\tau,\mathbf{x})$ in Fourier space and using the Wick theorem, we obtain

$$\langle \mathcal{R}_{\mathbf{k}_1}\mathcal{R}_{\mathbf{k}_2}\mathcal{R}_{\mathbf{k}_3}\rangle = \mathrm{Re}\left\{2i\,u^0_{\mathbf{k}_1}u^0_{\mathbf{k}_2}u^0_{\mathbf{k}_3}\int_{-\infty}^{0}\frac{d\tau}{\tau^2}\frac{\epsilon M_{\rm Pl}^2}{H^2}(2\pi)^3\int d^3q_1\int d^3q_2\int d^3q_3\,\delta(\mathbf{q}_1+\mathbf{q}_2+\mathbf{q}_3)\right.$$

$$\times\Big[4sc_s^{-2}u^*_{\mathbf{q}_1}(\tau)u^{*\prime}_{\mathbf{q}_2}(\tau)u^{*\prime}_{\mathbf{q}_3}(\tau)\Big(\delta(\mathbf{k}_1-\mathbf{q}_1)\delta(\mathbf{k}_2-\mathbf{q}_2)\delta(\mathbf{k}_3-\mathbf{q}_3)+\{\mathbf{k}_1\leftrightarrow\mathbf{k}_2\}+\{\mathbf{k}_1\leftrightarrow\mathbf{k}_3\}\Big)$$

$$-6\tau\left(1-c_s^{-2}\right)u^{*\prime}_{\mathbf{q}_1}(\tau)u^{*\prime}_{\mathbf{q}_2}(\tau)u^{*\prime}_{\mathbf{q}_3}(\tau)\delta(\mathbf{k}_1-\mathbf{q}_1)\delta(\mathbf{k}_2-\mathbf{q}_2)\delta(\mathbf{k}_3-\mathbf{q}_3)$$

$$-2\tau\left(1-c_s^{-2}\right)(\mathbf{q}_2\cdot\mathbf{q}_3)\,u^{*\prime}_{\mathbf{q}_1}(\tau)u^{*}_{\mathbf{q}_2}(\tau)u^{*}_{\mathbf{q}_3}(\tau)\Big(\delta(\mathbf{k}_1-\mathbf{q}_1)\delta(\mathbf{k}_2-\ \mathbf{q}_2)\delta(\mathbf{k}_3-\mathbf{q}_3)$$

$$\left.+\{\mathbf{k}_1\leftrightarrow\mathbf{k}_2\}+\{\mathbf{k}_1\leftrightarrow\mathbf{k}_3\}\Big)\Big]\right\}\,,$$

where $u^0_{\mathbf{k}_1} \equiv u_{\mathbf{k}_1}(0)$. For the leading order contribution, it suffices to use the zeroth-order mode function

$$u_{\mathbf{k}}(\tau) = \frac{iH}{\sqrt{4\epsilon c_{s,0} k^3}} \left(1 + ikc_{s,0}\tau\right) e^{-ikc_{s,0}\tau} \ , \tag{3.37}$$

and the three-point correlation function is then:

$$\begin{aligned}
\langle \mathcal{R}_{\mathbf{k}_1} \mathcal{R}_{\mathbf{k}_2} \mathcal{R}_{\mathbf{k}_3} \rangle = {} & \frac{\mathcal{P}^2_{\mathcal{R},0} (2\pi)^7 M_{\rm Pl}^6}{8 k_1^3 k_2^3 k_3^3} \delta(\mathbf{k}_1 + \mathbf{k}_2 + \mathbf{k}_3) \int_{-\infty}^0 d\tau \Big\{ \cos\left(K c_{s,0}\tau\right) \\
& \times \Big[4 s c_s^{-2} c_{s,0}^3 \tau k_1 k_2 k_3 (k_1 k_2 + 2 \text{ perm}) - 2\tau c_{s,0} \left(1 - c_s^{-2}\right) \left[k_1^2 (k_2 + k_3)(\mathbf{k}_2 \cdot \mathbf{k}_3) + 2 \text{ perm} \right] \Big] \\
& - \sin\left(K c_{s,0}\tau\right) \Big[4 s c_s^{-2} c_{s,0}^2 (k_1^2 k_2^2 + 2 \text{ perm}) - 6\tau^2 c_{s,0}^4 \left(1 - c_s^{-2}\right) k_1^2 k_2^2 k_3^2 - 2 \left(1 - c_s^{-2}\right) \\
& \times \left[k_1^2 (\mathbf{k}_2 \cdot \mathbf{k}_3) + 2 \text{ perm} \right] + 2\tau^2 c_{s,0}^2 \left(1 - c_s^{-2}\right) k_1 k_2 k_3 \left[k_1 (\mathbf{k}_2 \cdot \mathbf{k}_3) + 2 \text{ perm} \right] \Big] \Big\} \ ,
\end{aligned} \tag{3.38}$$

where $K \equiv k_1 + k_2 + k_3$ and $\mathcal{P}_{\mathcal{R},0} = H^2/(8\pi^2 \epsilon M_{\rm Pl}^2 c_{s,0})$. Before we proceed, some comments are in order:

- For steps in the potential, one also has to calculate the contribution to the three-point function coming from similar cubic operators. It is easy to track the polynomials in k_i arising from the different operators if one pays attention to the form of the mode functions (3.37). This way, we noticed that the result for steps in the potential in [113, eq. 3.32] is missing a term, so it should display as follows:

$$\begin{aligned}
\frac{\mathcal{G}}{k_1 k_2 k_3} = \frac{1}{4} \epsilon_{\rm step} \mathcal{D}\left(\frac{K\tau_f}{2\beta}\right) \Bigg[& \left(\frac{k_1^2 + k_2^2 + k_3^2}{k_1 k_2 k_3 \tau_f} - K\tau_f \right) K\tau_f \cos(K\tau_f) \\
& - \left(\frac{k_1^2 + k_2^2 + k_3^2}{k_1 k_2 k_3 \tau_f} - \frac{\sum_{i \neq j} k_i^2 k_j}{k_1 k_2 k_3} K\tau + K\tau \right) \sin(K\tau_f) \Bigg]
\end{aligned} \tag{3.39}$$

  This is indeed good news, since the missing term ($+K\tau$) above was the source of a small discrepancy found by the authors of [113] with respect to previous results [124], of order $10 - 15\%$ on large scales. We have checked that this discrepancy vanishes when the extra term is introduced.

- We consider sharp features ($\beta_s \gg 1$) peaking in τ_f and define the new variable y through $\tau = \tau_f \, e^{-y/\beta_s}$, as we did for the power spectrum. There are two kinds of functions appearing in equation (3.38): polynomials and oscillating functions. For the latter, we substitute $\tau \simeq \tau_f (1 - y/\beta_s)$ and do not expand further, in order

to keep the Fourier transforms. For the former, the zeroth order approximation $\tau \simeq \tau_f$ (as in [113]) provides excellent results[5], although we take the next order and evaluate them at $\tau \simeq \tau_f(1 - y/\beta_s)$ to test for not-so-sharp features. We will therefore calculate the first order correction to previous results. Furthermore we consider, apart from the operator $\mathcal{R}\dot{\mathcal{R}}^2$ (proportional to s), two extra contributions $\dot{\mathcal{R}}^3$ and $\dot{\mathcal{R}}(\nabla\mathcal{R})^2$ (proportional to u) and show that they all contribute at the same order, independently of the sharpness β_s. This is because, although s is proportional to the sharpness β_s, it is also proportional to the derivative of the shape function, F', defined in eq. (3.25). On the other hand, u is proportional to the shape function, but the Fourier transform of F introduces an additional factor β_s relative to the Fourier transform of F', cf. eqs. (3.27),(3.28) and (3.41)–(3.43).

- The integrals in (3.38) contain Fourier transforms of the shape function F and its derivative, given the definitions in eqs. (3.24) and (3.25). The symmetric and antisymmetric envelope functions arising from the Fourier transform of F' were already defined in equations (3.27) and (3.28). For completeness, we will give the complementary definitions obtained when integrating by parts:

$$\int_{-\infty}^{\infty} dy\, F(y) \cos\left(\frac{K c_{s,0}\tau_f}{\beta_s} y\right) = -\frac{\beta_s}{2K c_{s,0}\tau_f}\mathcal{D}_S \quad , \tag{3.40}$$

$$\int_{-\infty}^{\infty} dy\, F(y) \sin\left(\frac{K c_{s,0}\tau_f}{\beta_s} y\right) = \frac{\beta_s}{2K c_{s,0}\tau_f}\mathcal{D}_A \quad , \tag{3.41}$$

$$\int_{-\infty}^{\infty} dy\, y\, F(y) \cos\left(\frac{K c_{s,0}\tau_f}{\beta_s} y\right) = \frac{1}{2}\left(\frac{\beta_s}{K c_{s,0}\tau_f}\right)^2 \left(K\frac{d\mathcal{D}_A}{dK} - \mathcal{D}_A\right) \ , \tag{3.42}$$

$$\int_{-\infty}^{\infty} dy\, y\, F(y) \sin\left(\frac{K c_{s,0}\tau_f}{\beta_s} y\right) = \frac{1}{2}\left(\frac{\beta_s}{K c_{s,0}\tau_f}\right)^2 \left(K\frac{d\mathcal{D}_S}{dK} - \mathcal{D}_S\right) \ , \tag{3.43}$$

where the slight change of notation between these definitions and those in equations (3.27) and (3.28) is given by $K \leftrightarrow 2k$. We also imposed that F asymptotically vanishes when integrating by parts, which will be the case in this calculation.

Taking into account the comments above, we calculate the bispectrum to leading order for the particular case in which $c_{s,0} = 1$, so that we can compare to the SRFT method. We will express the bispectrum in terms of the normalized scale-dependent function

[5] As opposed to the power spectrum, in this case we only have polynomials with positive powers of $k\tau$, and therefore evaluating them at $k\tau_f$ is already a good approximation for sufficiently sharp features.

$f_{\rm NL}(\mathbf{k}_1,\mathbf{k}_2,\mathbf{k}_3)$ defined by:

$$\begin{aligned}\langle\mathcal{R}_{\mathbf{k}_1}\mathcal{R}_{\mathbf{k}_2}\mathcal{R}_{\mathbf{k}_3}\rangle &= (2\pi)^3\delta(\mathbf{k}_1+\mathbf{k}_2+\mathbf{k}_3)\Delta B_{\mathcal{R}}\\ &= (2\pi)^7\delta(\mathbf{k}_1+\mathbf{k}_2+\mathbf{k}_3)\frac{3}{10}f_{\rm NL}(\mathbf{k}_1,\mathbf{k}_2,\mathbf{k}_3)\mathcal{P}^2_{\mathcal{R},0}\frac{k_1^3+k_2^3+k_3^3}{k_1^3k_2^3k_3^3}\end{aligned} \qquad (3.44)$$

and we will use the following identities for a triangle of vectors $\{\mathbf{k}_1,\mathbf{k}_2,\mathbf{k}_3\}$:

$$\begin{aligned}k_1(\mathbf{k}_2\cdot\mathbf{k}_3)+2\text{ perm} &= \frac{1}{2}\left[k_1^3+k_2^3+k_3^3-K(k_1k_2+2\text{ perm})+3k_1k_2k_3\right]\ ,\\ k_1^2(\mathbf{k}_2\cdot\mathbf{k}_3)+2\text{ perm} &= \frac{1}{2}\left[k_1^4+k_2^4+k_3^4-2(k_1^2k_2^2+2\text{ perm})\right]\ ,\\ k_1^2(k_2+k_3)(\mathbf{k}_2\cdot\mathbf{k}_3)+2\text{ perm} &= \frac{1}{2}\left[K(k_1^4+k_2^4+k_3^4)-(k_1^5+k_2^5+k_3^5)-K(k_1^2k_2^2+2\text{ perm})\right.\\ &\quad\left.-k_1k_2k_3(k_1k_2+2\text{ perm})\right]\ .\end{aligned}$$

Finally, the bispectrum contribution due to variations in the speed of sound as considered in the cubic action (3.34), to first order in the size of the feature σ_*, and to first order in the polynomial expansion $\tau\simeq\tau_f(1-y/\beta_s)$ reads:

$$\begin{aligned}f_{\rm NL}(\mathbf{k}_1,\mathbf{k}_2,\mathbf{k}_3) &= \frac{5}{24}\frac{\sigma_*}{k_1^3+k_2^3+k_3^3}\times\left\{\cos(K\tau_f)\left\{\tau_f^2\,\frac{k_1k_2k_3}{K}\Big[(k_1^3+k_2^3+k_3^3)\right.\right.\\ &+K(k_1k_2+2\text{ perm})-3k_1k_2k_3\Big]\mathcal{D}_A+\frac{\tau_f}{K}\Big[K(k_1^4+k_2^4+k_3^4)-(k_1^5+k_2^5+k_3^5)\\ &+K(k_1^2k_2^2+2\text{ perm})-4k_1k_2k_3(k_1k_2+2\text{ perm})+3\frac{k_1k_2k_3}{K}(k_1^3+k_2^3+k_3^3)-9\frac{k_1^2k_2^2k_3^2}{K}\Big]\mathcal{D}_S\\ &-3\tau_f\frac{k_1k_2k_3}{K}\Big[(k_1^3+k_2^3+k_3^3)+\frac{1}{3}K(k_1k_2+2\text{ perm})-3k_1k_2k_3\Big]\frac{d\mathcal{D}_S}{dK}\\ &-\frac{1}{K^2}\Big[3K(k_1^4+k_2^4+k_3^4)-2(k_1^5+k_2^5+k_3^5)-4K(k_1^2k_2^2+2\text{ perm})\\ &-2k_1k_2k_3(k_1k_2+2\text{perm})\Big]\mathcal{D}_A+\frac{1}{K}\Big[2K(k_1^4+k_2^4+k_3^4)-2(k_1^5+k_2^5+k_3^5)\\ &\left.-2k_1k_2k_3(k_1k_2+2\text{perm})\Big]\frac{d\mathcal{D}_A}{dK}-\frac{1}{\tau_fK^2}\Big[(k_1^4+k_2^4+k_3^4)-2(k_1^2k_2^2+2\text{ perm})\Big]\left(\mathcal{D}_S-K\frac{d\mathcal{D}_S}{dK}\right)\right\}\\ &+\sin(K\tau_f)\left\{\{\mathcal{D}_S\leftrightarrow\mathcal{D}_A\ ,\ \tau_f\leftrightarrow-\tau_f\}\right\}\Bigg\}\ ,\end{aligned} \qquad (3.45)$$

where the $\sin(K\tau_f)$ in the last line contains the same terms as the $\cos(K\tau_f)$, but changing $\mathcal{D}_S\leftrightarrow\mathcal{D}_A$ and $\tau_f\leftrightarrow-\tau_f$, as indicated. This is the formula we want to compare with equation (3.6), after proper normalization. Below, we show the comparison for different

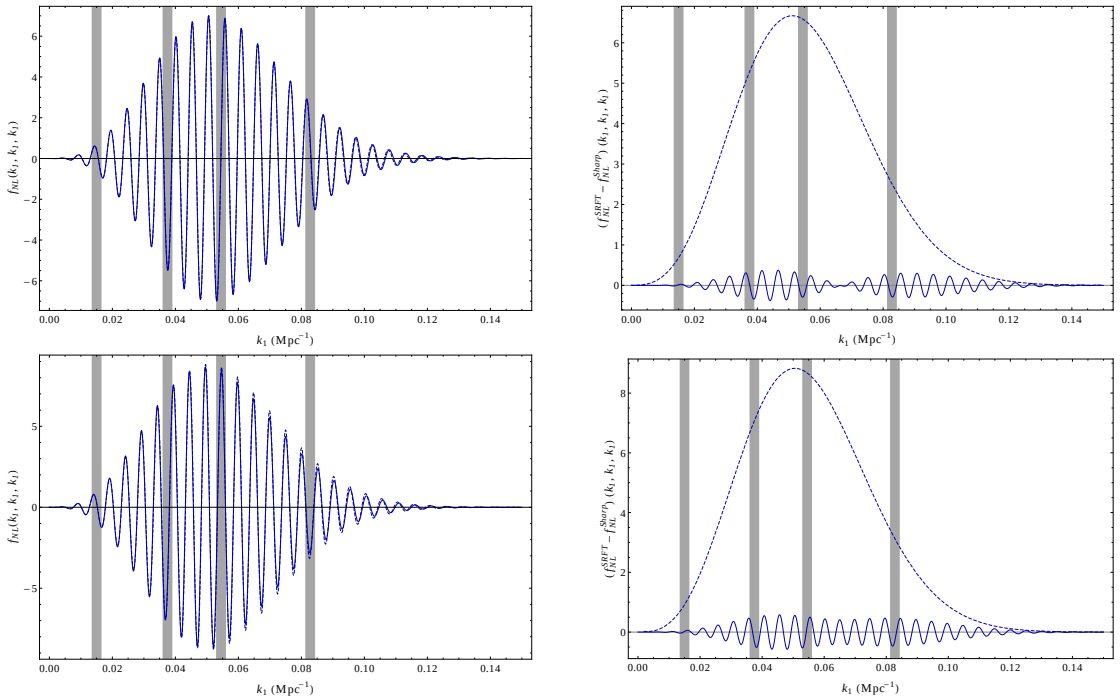

FIGURE 3.4: *left*: bispectrum $f_{\rm NL}$ signal in the equilateral limit with the normalization indicated in eq. (3.44), given by a symmetric reduction in the speed of sound as in (3.46) (*top*) and an asymmetric reduction as in (3.48) (*bottom*), calculated with the SRFT formula (3.6) (solid) and with the sharp approximation (3.45) (dashed). *right*: absolute difference between the signals showed in the left plot (solid), together with the envelope of the signal (dashed). The grey strips represent the approximate scales of the first four acoustic peaks of the CMB temperature spectrum. The parameters are $\sigma_* = 0.04$, $\beta_s = 25.5$, $\ln(-\tau_f) = 6$. This gives $|s|_{\rm max} \simeq 0.42$ for the symmetric case and $|s|_{\rm max} \simeq 0.55$ for the asymmetric case. In both cases the relative difference with respect to the envelope is large only at very small scales, which will be indistinguishable at the observational level. We are also within the limit $|s|_{\rm max} < 1$, where these signatures are reliable but sharp enough so that the sharp approximation works.

functional forms of the speed of sound.

3.2.5 Comparison of bispectra

In this section we compare the bispectrum obtained using the SRFT method (3.6) with that using the first order approximation for sharp features (3.45). As a first example, one can reproduce our test case of gaussian reductions in the speed of sound, cf. equation (3.51), by taking:

$$F = \exp\left[-\beta_s^2\left(\ln\frac{\tau}{\tau_f}\right)^2\right] \quad \Rightarrow \quad 1 - c_s^{-2} = -\sigma_*\, e^{-\beta_s^2\left(\ln\frac{\tau}{\tau_f}\right)^2} + \mathcal{O}\left(\sigma_*\right)^2 \,, \tag{3.46}$$

where the correspondence between this set of parameters and the one used in [156] is $\sigma_* \leftrightarrow -B$, $\tau_f \leftrightarrow \tau_0$, and $\beta_s \leftrightarrow \sqrt{\beta}$. In this case F is symmetric in the variable $y = -\beta_s \ln\frac{\tau}{\tau_f}$ and therefore only the symmetric envelope function $\mathcal{D}_S$ contributes, which

is given by

$$\mathcal{D}_S = -\frac{2K\tau_f}{\beta_s}\sqrt{\pi}\exp\left(-\frac{K^2\tau_f^2}{4\beta_s^2}\right) \quad , \quad \mathcal{D}_A = 0 \ . \tag{3.47}$$

In figure 3.4 we show the excellent agreement between the results obtained with equations (3.6) and (3.45) for the equilateral limit $k_1 = k_2 = k_3$. We have checked that for other configurations in momentum space, such as the folded or the squeezed shapes, the agreement is very similar. Note that in figure 3.4 we are plotting the absolute difference in $f_{\rm NL}$ and comparing with the total envelope of the signal[6]. At small scales one can see that the relative difference compared to the total signal is high, due to the fact that the approximation for sharp features starts to fail for large values of $K\tau$. However, the absolute signal is insignificant at such small scales.

As a second example, we propose a shape function with an antisymmetric part:

$$F = \exp\left[-\beta_s^2\left(\ln\tfrac{\tau}{\tau_f}\right)^2 + \beta_s \ln\tfrac{\tau}{\tau_f}\right] \ , \tag{3.48}$$

so that

$$1 - c_s^{-2} = -\sigma_* \left(\frac{\tau}{\tau_f}\right)^{\beta_s} e^{-\beta_s^2\left(\ln\frac{\tau}{\tau_f}\right)^2} + \mathcal{O}\left(\sigma_*\right)^2 \ . \tag{3.49}$$

Then, the symmetric and antisymmetric envelope functions read

$$\mathcal{D}_S = -\frac{2K\tau_f}{\beta_s}\sqrt{\pi}\exp\left(\frac{\beta_s^2 - K^2\tau_f^2}{4\beta_s^2}\right)\cos\left(\frac{K\tau_f}{2\beta_s}\right) \quad ,$$

$$\mathcal{D}_A = -\frac{2K\tau_f}{\beta_s}\sqrt{\pi}\exp\left(\frac{\beta_s^2 - K^2\tau_f^2}{4\beta_s^2}\right)\sin\left(\frac{K\tau_f}{2\beta_s}\right) . \tag{3.50}$$

We show in figure 3.4 the equilateral bispectrum signal produced by the asymmetric shape given by eq. (3.48), again derived using equations (3.6) and (3.45). As one can see in figure 3.4, the agreement is also remarkable for functions with an antisymmetric part.

3.3 Search for features in the Planck data

Equipped with accurate analytical predictions for the effect of a varying speed of sound in the power spectrum and bispectrum, we are in a position to search for these features in the CMB data. We choose to parametrize the reduction in the speed of sound as a

[6]We point out that the total envelope of the signal is not given by $\mathcal{D}_S$ or $\mathcal{D}_A$ alone. The total envelope is a combination of both functions, their derivatives, and the polynomials of k_i that appear in Equation 3.45.

gaussian in e-folds N as previously defined in eq. (3.33), i.e.

$$u = 1 - c_s^{-2} = B\, e^{-\beta(N-N_0)^2} = B\, e^{-\beta\left(\ln\frac{\tau}{\tau_0}\right)^2}\,, \tag{3.51}$$

where $\beta > 0$, $B < 0$ and N_0 (or τ_0) is the instant of maximal reduction. Assuming slow-roll, $\ln(-\tau) = (N_{\rm in} - N) - \ln(a_{\rm in}H_0)$, where $a_{\rm in} = a(N_{\rm in})$ and $N_{\rm in}$ is the time when the last ~ 60 e-folds of inflation start.

This functional form is inspired by soft turns along a multi-field inflationary trajectory with a large hierarchy of masses, a situation that is consistently described by an effective single-field theory [55, 76, 81, 92] (see also [82, 131]). Here, the value of the speed of sound asymptotes to one at the beginning and at the end of inflation (as opposed to step features in which the value at the beginning and at the end of inflation are different). Nevertheless we stress that reductions in the speed of sound are a more general phenomenon within effective field theory (and hence may have diverse shapes and physical origins).

3.3.1 Parameter space

The template for the speed of sound feature (3.51) has three parameters, namely B (the amplitude), β (the sharpness) and τ_0 (equivalently N_0, the time of maximum reduction). There are two main criteria that we followed in order to determine the explored parameter regions:

(a) The angular scales probed by Planck ($\ell = 2 - 2500$) roughly correspond to certain momentum scales crossing the Hubble sound horizon during the first $N_{\rm CMB} \simeq 7$ e-folds of the last ~ 60 e-folds of inflation. If the data resembles features due to a reduced speed of sound, it is most likely to find them in this "CMB window". The sharpness β and the position N_0 are chosen so that the reduction happens well within this window[7]. As a by-product, we avoid degeneracies with the spectral index n_s and the optical depth $\tau_{\rm reio}$ that would be present in very wide reductions.

(b) The Slow Roll Fourier Transform (SRFT) calculation of the power spectrum and the bispectrum (reviewed in section 3.2.1) is valid for mild and moderately sharp reductions of the speed of sound. Also, the slow-roll contributions to the bispectrum are disregarded with respect to the terms arising from the reduced speed of sound [108]. This means that the amplitude $|u|$ and the rate of change $s \equiv \frac{\dot{c}_s}{c_s H}$ must be much smaller than one, while being (at least one of them) much larger than

[7] As we explain later, this a sufficient but not necessary condition for inducing changes in the power spectrum at these scales.

the slow-roll parameters. More precisely we demand the following hierarchy to be present

$$\mathcal{O}(\epsilon,\eta) \ll \text{Max}\,(|u|,|s|) \ll 1\ . \tag{3.52}$$

We took a very conservative definition for the total width of the reduction (in e-folds): ten standard deviations, $\Delta N = 10/\sqrt{2\beta}$. Then, from **(a)**, the position N_0 and the sharpness β should satisfy $5\sqrt{2\beta} < N_0 < N_{\rm CMB} - 5\sqrt{2\beta}$ and $10\sqrt{2\beta} < N_{\rm CMB}$. As to the perturbative regime, the rate of change s of the speed of sound (3.51) reads:

$$s(N) = \frac{1}{c_s}\frac{dc_s}{dN} = -\frac{B\beta(N-N_0)\,e^{-\beta(N-N_0)^2}}{1-B\,e^{-\beta(N-N_0)^2}}\ . \tag{3.53}$$

Since we have to impose $|s| \ll 1$ for all values of N, it suffices to impose this condition at the point where $|s|$ takes its maximum value $|s(N_*)| = |s|_{\rm max}$, determined by:

$$N_* = N_0 \pm \frac{1}{\sqrt{2\beta}}\sqrt{1+\mathcal{O}(B)}\ \simeq\ N_0 \pm \frac{1}{\sqrt{2\beta}}\ , \tag{3.54}$$

which approximately corresponds to one standard deviation of our gaussian, and we have used that $|B| \ll 1$. Then the condition $|s|_{\rm max} \ll 1$ translates into $\beta \ll \frac{2e}{B^2} + \mathcal{O}(B^{-1})$. Altogether, the allowed region of our parameter space is taken to be:

$$\mathcal{O}(\epsilon,\eta) \ll |B| \ll 1\ , \tag{3.55a}$$

$$\frac{50}{N_{\rm CMB}^2} < \beta \ll \frac{2e}{B^2}\ , \tag{3.55b}$$

$$\frac{5}{\sqrt{2\beta}} < N_0 < N_{\rm CMB} - \frac{5}{\sqrt{2\beta}}\ . \tag{3.55c}$$

Notice that, as explained above in **(b)**, the bound $|B| \gg \mathcal{O}(\epsilon,\eta)$ can be avoided if $|s|_{\rm max} \gg \mathcal{O}(\epsilon,\eta)$. For computational purposes, we use the parameter $\ln(-\tau_0)$ instead of N_0 for the data analysis. We take uniform priors on B, $\ln\beta$ and $\ln(-\tau_0)$. The range for the parameter $\ln(-\tau_0)$ is taken to be more strongly restricted than by equation (3.55c):

$$4.4 \le \ln(-\tau_0) \le 6\ , \tag{3.56}$$

Before we proceed with the search in the data, a few comments are in order. The chosen region of parameter space (3.55) is a very conservative choice. First, equation (3.55c) and the lower bound in equation (3.55b) are more restrictive than the condition that the feature be observable. For example, we expect observable effects when the reduction occurs before the CMB window, since it would effectively modify the initial conditions of the modes subsequently leaving the sound horizon. We are also trying to avoid very broad features that could be degenerate with cosmological parameters as the spectral

index n_s and the optical depth $\tau_{\rm reio}$, as well as highly oscillating features (for large values of $|\tau_0|$) that make computational control difficult.

Secondly, this range is well within the region of the parameter space where the theory is weakly coupled. As we explained in Chapter 2 following [97], a hard upper bound on the sharpness of the feature can be derived by imposing that the theory is weakly coupled at the energy scale where the changes in the mode functions are induced. Our sharpness parameter β is related to that of [97] (that we will call $\beta_{\rm CBM}$) by $\beta = 50\beta_{\rm CBM}^2$, where we took the conservative definition of the width to be ten standard deviations. The feature unitarity bound eq. (2.88) imposes that our sharpness parameter must satisfy:

$$\ln\beta < 14 \ . \tag{3.57}$$

Since we restrict our search to $2 < \ln\beta < 7.5$, we are perfectly consistent with the bound given above. Even if we take the crude definition for the width of only one standard deviation, the correspondence would be $\beta = \beta_{\rm CBM}^2$, and the bound would translate to $\ln\beta < 10$, which still leaves us in a safe region. Given that we *a priori* constrained our search to a region of the parameter space where the perturbative and adiabatic regimes are respected, the predictions obtained are consistently interpreted by the underlying theory.

Let us note that respecting the weak coupling condition (3.57) has important consequences. Indeed, it was found [97, 98] that some of the best fits found so far for steps in the potential in the CMB [136, 146, 147] do not lie within this bound. This calls into question the consistency of the framework in which these predictions are derived. More interestingly, this motivates a new theoretical framework able to consistently describe those predictions, since the data is blind to whether a theory is internally consistent or not. An important and evident conclusion of these analyses is that very sharp features are problematic from the theoretical point of view. In addition, one could speculate that if the data finally points to inflationary scenarios with large field excursions, a (slightly broken) symmetry should protect the background, and then we would not expect to find sharp features in the potential. This further motivates the study of moderately sharp features, which are still safely described by an underlying theory. In the following, we present the results of our search.

3.3.2 Results

As already stated in precedent section, a variation in the speed of sound will generate a primordial power spectrum given by:

$$\frac{\Delta\mathcal{P}_{\mathcal{R}}}{\mathcal{P}_{\mathcal{R},0}}(k) = k\int_{-\infty}^{0} d\tau\ u(\tau)\sin(2k\tau)\ , \tag{3.58}$$

This primordial power spectrum feature is computed using a Fast Fourier Transform, and added to the primordial spectrum of the ΛCDM Planck baseline model described in ref. [157, sec. 2]. The resulting CMB power spectrum, calculated using the CLASS Boltzmann code [29, 158], is fitted to the Planck 2013 CMB temperature data [159] and the WMAP CMB low-ℓ polarization data [160], using MONTE PYTHON [161] as a Markov chain Monte Carlo (MCMC) sampler. We varied all cosmological, nuisance and feature parameters. For those last ones, the likelihood probability distribution is found to be multi-modal. Though multi-modal distributions are more efficiently sampled using other methods (e.g. MULTINEST [162, 163]), we were able to perform the search using only MCMC's.

Our statistical analysis of the Planck CMB power spectrum reveals several fits with a moderately improved likelihood compared to the best ΛCDM fit. Having discarded small signals with $\Delta\chi^2 > -2$ (defined in [8]) over ΛCDM, we find a series of five well-isolated bands of almost constant $\ln(-\tau_0)$, with variable significance, see table 3.1 and figure 3.5. For each of those fits we give the associated full primordial bispectrum. At the time of writing this thesis the Planck bispectrum data have not yet been released, but templates similar to our predictions have already been tested by the Planck collaboration. We find, through a heuristic and limited comparison, that the predicted bispectra have frequencies which are not favoured by the latest data.

The amplitude B of the fits is rather small, $\mathcal{O}(10^{-2})$, and therefore comparable with neglected slow-roll terms. This means the bispectrum is dominated by terms of order $s = \dot{c}_s/(Hc_s)$. The maximum values of s at the best fits for the modes $\mathcal{A}$ to $\mathcal{E}$ in table 3.1 are respectively 0.33, 0.42, 0.40, 0.48, 0.05. Notice that the value of s for $\mathcal{E}$ is also comparable to neglected terms, so the prediction for the bispectrum based on eq. (3.6) cannot be trusted in this case. We therefore disregard this mode in the comparison with the bispectrum.

For the modes $\mathcal{A}$, $\mathcal{B}$ and $\mathcal{C}$ the table shows the 68% c.l. ranges. For bands $\mathcal{B}$ and $\mathcal{C}$ we were unable to put an upper bound on $\ln\beta$ due to a degeneracy between that parameter

[8] Hereafter, χ^2 refers to the *effective* quantity defined as $\chi^2_{\text{eff}} = -2\ln\mathcal{L}$, see [164, p. 10]; in turn, Δ stands for the difference with the corresponding best fit value of Planck baseline model, using the same likelihood.

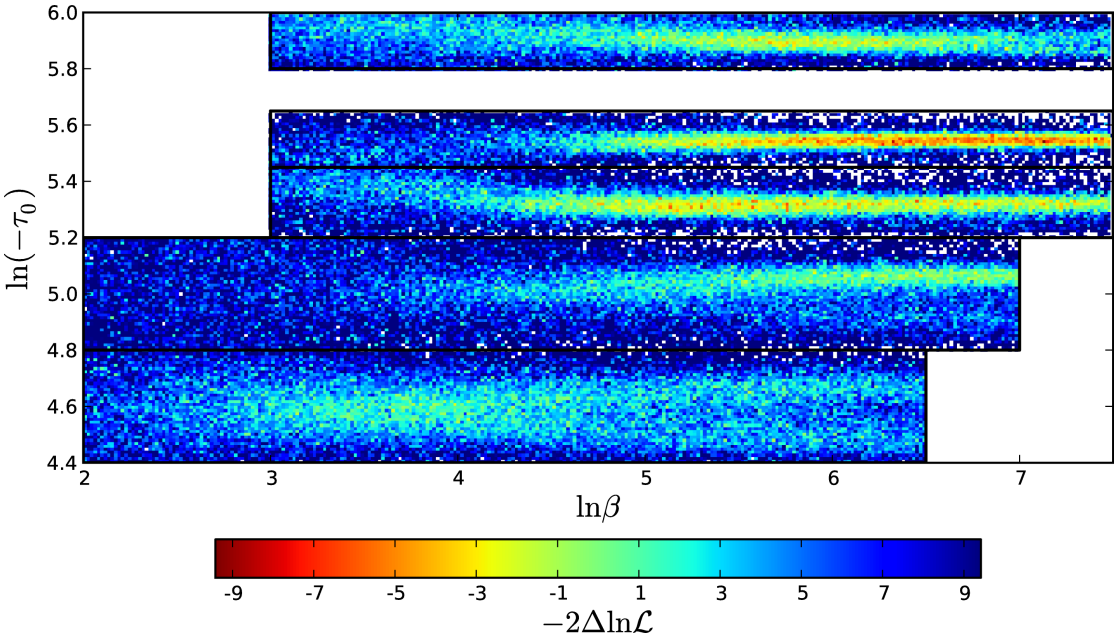

FIGURE 3.5: Profile of $\Delta\chi^2_{\rm eff} = -2\Delta\ln\mathcal{L}$ for the features in the CMB power spectrum in the $(\ln\beta,\, \ln(-\tau_0))$ plane.

#	$-B\times 10^2$	$\ln\beta$	$\ln(-\tau_0)$	$\Delta\chi^2$
$\mathcal{A}$	$(4.5)\, 3.7\,^{+1.6}_{-3.0}$	$(5.7)\, 5.7\,^{+0.9}_{-1.0}$	$(5.895)\, 5.910\,^{+0.027}_{-0.035}$	-4.3
$\mathcal{B}$	$(4.2)\, 4.3\,\pm 2.0$	$(6.3)\, 6.3\,^{+1.2}_{-0.4}$	$(5.547)\, 5.550\,^{+0.016}_{-0.015}$	-8.3
$\mathcal{C}$	$(3.6)\, 3.1\,^{+1.6}_{-1.9}$	$(6.5)\, 5.6\,^{+1.9}_{-0.7}$	$(5.331)\, 5.327\,^{+0.026}_{-0.034}$	-6.2
$\mathcal{D}$	(4.4)	(6.5)	(5.06)	-3.3
$\mathcal{E}$ *	(1.5)	(4.0)	(4.61)	-2.2

TABLE 3.1: CMB power spectrum best fits (in parentheses), 68% c.l. intervals and effective $\Delta\chi^2$ at the best fit value for each of the different modes. The prediction for the bispectrum for $\mathcal{E}$ is not reliable (see text).

and the amplitude $|B|$. For those two modes, the upper bound on $\ln\beta$ is set by the prior $s < 1$ in eq. (3.55b), which is saturated at $\ln\beta \simeq 7.5$. The best fit for $\mathcal{B}$ lies at $s \simeq 1$, so we present in table 3.1 the second best[9]. We show in figure 3.6 the predicted C_l for mode $\mathcal{B}$.

The lower bands $\mathcal{D}$ (and $\mathcal{E}$) are less significant and their likelihoods much less gaussian, so we only show their best fits. Despite their low significance, they are worthy of mention because they fall in the region overlapping with Planck's search for features in the bispectrum (see below).

The best fits and 68% c.l. ranges [157] of the six ΛCDM parameters are quite accurately reproduced. We find two mild degeneracies ($|r| \lesssim 0.15$) of $\ln(-\tau_0)$ with $\omega_{\rm CDM}$ and H_0.

[9]The high-ℓ CMB polarization data of the new Planck release should put an upper bound on $\ln\beta$, as well as confirm that we are not fitting noise. This is an important reason for repeating this analysis with the new data.

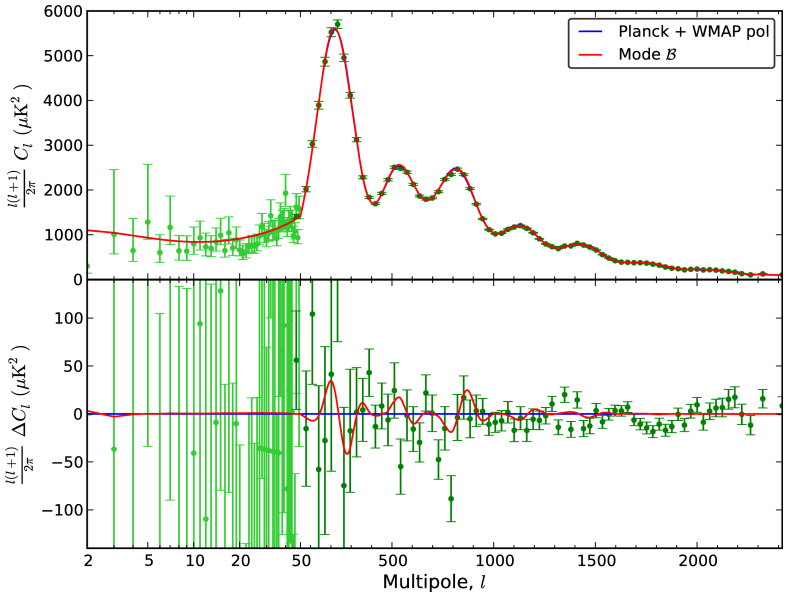

FIGURE 3.6: CMB temperature power spectrum for mode $\mathcal{B}$.

Best fits and confidence intervals are also preserved for the nuisance parameters.

Due to the Fourier transform in eq. (3.58), our features oscillate as $\exp(i2k\tau_0)$. Thus it is natural to compare to other searches for linearly oscillating features in the Planck CMB power spectrum[10]. In [145], Meerburg et al. searched for constant amplitude oscillations with frequencies that compare to ours as $\omega_2 = 2|\tau_0|$. The search was done up to $\ln(-\tau_0) = 9$. In the overlapping region, $\omega_2 \in [160, 810]$, they find peaks at roughly $\ln(-\tau_0) \sim \{5.0, 5.1, 5.3, 5.6, 5.7\}$ ($|\Delta\chi^2_{\rm bf}| \simeq 8$). We find three peaks in this region with similar significance; it could be that the discrepancies come from signals at scales at which our (localized) features are negligible.

Also, the Planck collaboration [146, sec. 8] searched for features motivated by step-inflation [135]. In 2013 they performed a search up to frequency $\ln(-\tau_0) = 12$ (in that parametrization $\eta_f = |\tau_0|$). The profile likelihood in [146, fig. 19, middle] reveals peaks at $\ln \eta_f \in [4.5, 4.8]$ ($|\Delta\chi^2_{\rm bf}| \simeq 2$) and $\ln \eta_f \in [5.3, 5.7]$ ($|\Delta\chi^2_{\rm bf}| \simeq 8$), which is consistent with our results. It is worth noting that in both searches above (also in [147]) the overall best fit occurs at $\ln(-\tau_0) \simeq 8.2$ ($|\Delta\chi^2_{\rm bf}| \sim 10$), too high a frequency for the scope of our search.

Our analysis and the ones mentioned above were made with the 2013 Planck data. Since that date new data became available, in particular containing new polarization measurements. At the moment only the Planck collaboration has repeated the analysis [30], containing a new search for both step features and linear oscillations. For steps in the potential the best fit value reaches a maximum of $|\Delta\chi^2_{\rm bf}| \sim 8$ for a slightly

[10] Logarithmic oscillations, in which the primordial power spectrum oscillates as $\cos(\omega \ln(k))$, is also a well studied and motivated template (see [30] and references therein).

smaller frequency ($\ln(-\tau_0) \simeq 7.1$) and different values for the amplitude and width of the envelope (the fit is similar to the one found by Benetti in [136]).

In all the cases mentioned above (and also including searches with templates with fewer parameters), the bayesian evidence does not prefer the feature model over the featureless power law spectra, which suggests that CMB power spectrum data alone cannot justify the introduction of these features. Nevertheless, one of the aims of this chapter is to show that low-significance fits can still predict correlated features in the bispectrum which are possibly observable with the current data. Model selection should be done taking into account both observables (or naturally, any other combination).

3.3.3 Comparison with the search for features in Planck's bispectrum

A first search for linearly oscillatory features was performed on Planck's bispectrum with the 2013 data (cf. [165, sec. 7.3.3]) using a constant feature model (i.e. with no envelope modulating the amplitude of the oscillation). The constant feature template is given by [166]

$$B(k_1, k_2, k_3) = \frac{6A^2 f_{\rm NL}^{\rm feat}}{(k_1 k_2 k_3)^2} \sin\left(2\pi \frac{\sum_{i=1}^{3} k_i}{3k_c} + \phi\right) , \tag{3.59}$$

where $A = A_s k_*^{1-n_s}$, A_s and n_s being the amplitude and spectral index of the primordial power spectrum, and $k_* = 0.05$ Mpc^{-1} a pivot scale. They sampled the amplitude $f_{\rm NL}^{\rm feat}$ over a coarse grid of wavelengths k_c and phases ϕ. Our features also present a linearly oscillatory pattern, which comes from the Fourier transform in (3.5). These oscillations enter the bispectrum approximately as $\exp(i\sum_i k_i\tau_0)$, cf. eq. (3.6). Thus, Planck's 2013 search falls inside $\ln(-\tau_0) \in [4.43, 5.34]$, while ours spans up to $\ln(-\tau_0) = 6$ $\left(k_c = 0.00519 \text{ Mpc}^{-1}\right)$. The overlap includes our modes $\mathcal{C}$ and $\mathcal{D}$ (and also the discarded $\mathcal{E}$). In the range of $\ln(-\tau_0)$ probed here, we were not able to reproduce the improvement Planck appears to see for features at the first peak. On the other hand, we found good matching around the second and third peak scales between the best fit of $\mathcal{D}$ with $k_c = 0.01327$ Mpc^{-1} and the 2.3σ signal of Planck bispectrum at $k_c = 0.01375$ Mpc^{-1} with $f_{\rm NL}^{\rm feat} = 345$ and $\phi = \pi/2$.

Having found an interesting hint for the presence of such a feature, it is important to know whether such good matching persists when considering additional data. In particular, the Planck search for features in the bispectrum was extended in 2015 [40]. New feature templates were tested, and the search was enlarged to higher frequencies (up to $\ln(-\tau_0) = 7.6$ for the constant feature model, and therefore covering all the modes $\mathcal{A}$ to $\mathcal{E}$). Comparing our fits of the power spectrum with the new bispectrum search would require computing the best fit parameters for the power spectrum again, using

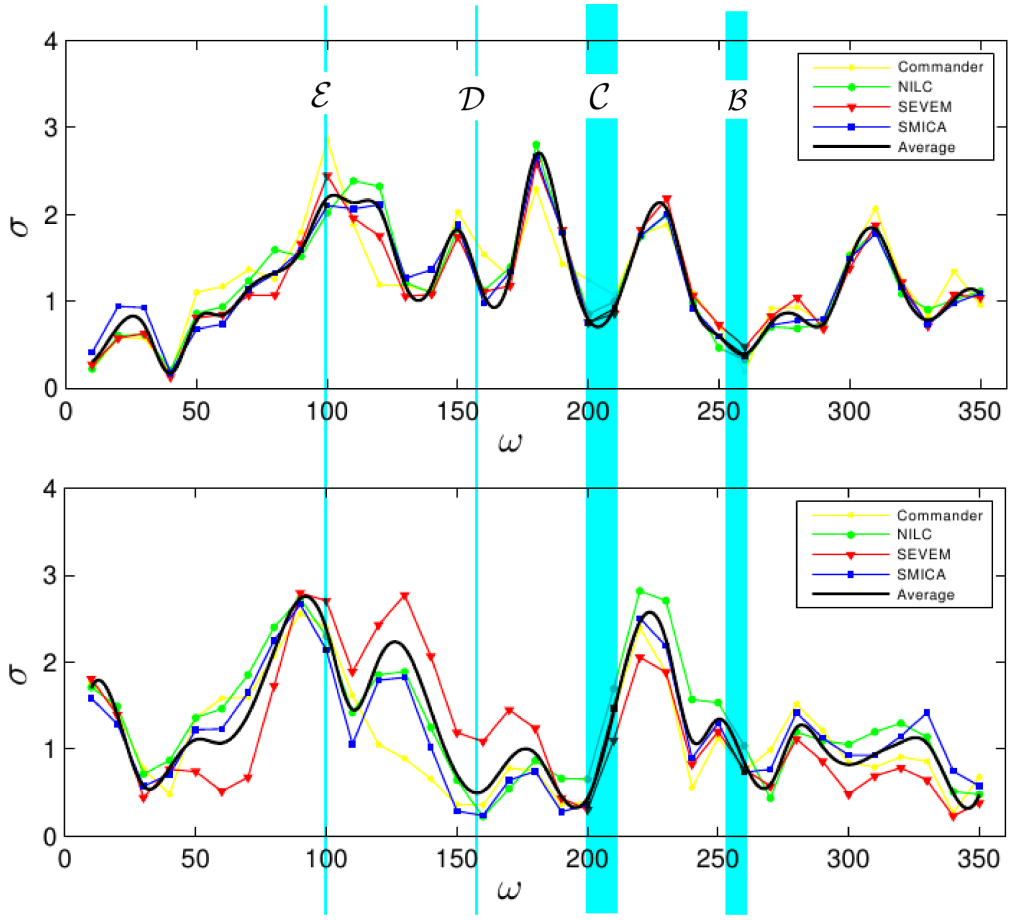

FIGURE 3.7: The likelihood for the constant feature models eq. (3.59), from Planck 2015 analysis [40]. Upper panel is for T only, and lower pannel is T+E. We superimpose in turquoise the best-fits frequencies we found in the power spectrum with the 2013 data.

the new released data. This is going to be done in the future, and for the moment we will very qualitatively address what happens for the fits found with the 2013 data.

In order to facilitate the comparison we write in table 3.2 our power spectrum fits in terms of the frequency ω defined as $\omega \equiv 2\pi/3k_c$ $(= -\tau_0)$. In figure (3.7) we show the

mode	$\mathcal{A}$	$\mathcal{B}$	$\mathcal{C}$	$\mathcal{D}$	$\mathcal{E}$
ω	$(363)\,369\,^{+10}_{-13}$	$(256)\,257\,^{+4}_{-4}$	$(207)\,206\,^{+5}_{-7}$	158	100

TABLE 3.2: CMB power spectrum best fits (parentheses) and 68% c.l. intervals for modes $\mathcal{A}$ to $\mathcal{E}$ (shown in table 3.1) in terms of the frequency $\omega = 2\pi/3k_c = -\tau_0$.

likelihood for the template (3.59) up to $\omega = 350$ (where there is a better resolution of the data). We superimpose to this figure the frequencies we found in the 2013 power spectrum.

For templates with both oscillations and envelopes, the case of a step in the speed of sound and a step in the slow-roll parameters were analyzed. While the full shape is given

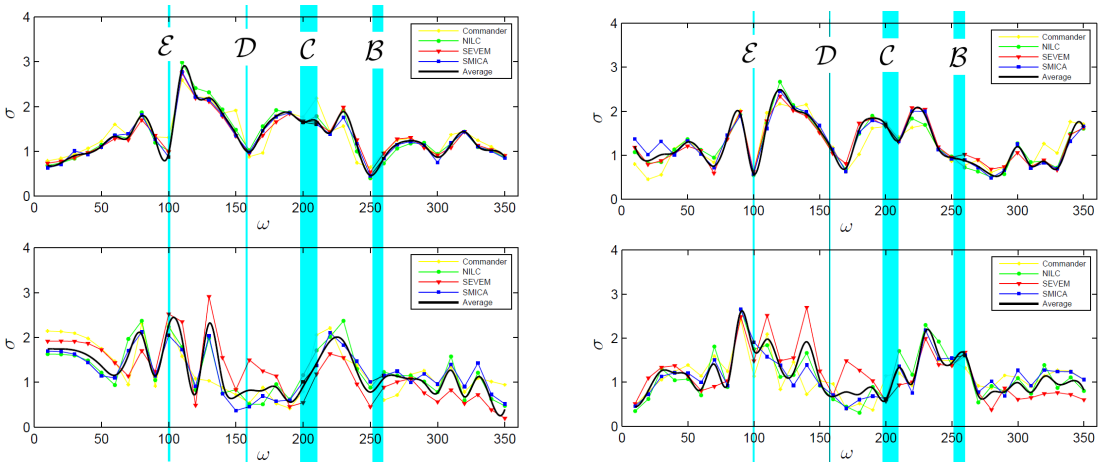

FIGURE 3.8: The likelihood for single feature models, whose dominant contribution is given in eqs. (3.60)-(3.61), from Planck 2015 analysis [40]. We superimpose in turquoise the best-fits frequencies we found in the power spectrum with the 2013 data. LEFT: Step in the potential (T-only top, and T+E bottom) RIGHT: Step in the speed of sound (T-only top, and T+E bottom).

by a very long formula, we can write the dominant contribution for each case. They are given by:

$$B_{K\sin}(k_1,k_2,k_3) = \frac{6A^2 f_{\rm NL}^{\rm feat}}{(k_1k_2k_3)^2} K\mathcal{D}(\alpha\omega K)\sin\left(2\pi\frac{\sum_{i=1}^3 k_i}{3k_c}+\phi\right)\,, \tag{3.60}$$

$$B_{K^2\cos}(k_1,k_2,k_3) = \frac{6A^2 f_{\rm NL}^{\rm feat}}{(k_1k_2k_3)^2} K^2\mathcal{D}(\alpha\omega K)\cos\left(2\pi\frac{\sum_{i=1}^3 k_i}{3k_c}+\phi\right)\,. \tag{3.61}$$

Here $f_{\rm NL}^{\rm feat}$ is a constant that sets the overall amplitude of the bispectrum, $\mathcal{D}(\alpha\omega)$ is the envelope function that modulates this amplitude in k-space, α is the sharpness of the step, and $K = k_1 + k_2 + k_3$. The envelope is taken to come from a tanh-step, i.e. $\mathcal{D}(\alpha\omega K) = \alpha\omega/\left(K\sinh(\alpha\omega K)\right)$ (see eq. (3.32)). We show the likelihood for these models as a function of the frequency of oscillation ω in figure 3.8.

From figures (3.7) and (3.8) we can see that only mode $\mathcal{E}$ correspond to a frequency that is a peak in the bispectrum ($\sigma \sim 2$ for all the envelopes). Some comments are in order. The likelihood values of figure (3.8) are obtained after marginalizing over the envelope factor α and the amplitude $f_{\rm NL}^{\rm feat}$. In our case they are not free parameters of the bispectrum since they are fixed by the fit to the power spectrum. Unfortunately we do not know how the likelihood changes as we vary these parameters. The likelihood values of figure (3.8) should then be understood as a maximum value for an arbitrary α and $f_{\rm NL}^{\rm feat}$. Furthermore, our template does not really correspond to any of the templates studied by Planck: while they considered a step in the speed of sound, i.e. an antisymmetric function, our test case is a symmetric reduction in the speed of sound. We know that the symmetry of the feature determines where does the envelope peaks, see e.g. figure

3.1, so this might be an important difference between our template and theirs. Whether the data can distinguish between these two templates is a question left for future work.

3.4 Conclusions

In this chapter we have studied moderately sharp features in the speed of sound from the point of view of theory and observations. In particular, we have shown that the effect of a transient reduction in the speed of sound can be calculated with the simple Slow Roll Fourier Transform (SRFT) approximation [108], in which the correlations between power spectrum and bispectrum are manifest. Additionally, we have presented an alternative way to calculate both the power spectrum and bispectrum, by consistently applying an approximation for moderately sharp features, both to the Generalized Slow Roll (GSR) power spectrum (eq. (3.29)) and to the in-in calculation of the bispectrum (eq. (3.45)). Within this regime, we have extended existing GSR calculations of the power spectrum to less sharp and arbitrary shapes of the speed of sound, and found excellent agreement with the SRFT approximation in the regime where both methods apply. Given that the regimes of validity of the two methods are not entirely coincident, we are now equipped with a robust machinery that will allow us to describe features in the speed of sound for a broader region of the parameter space. Broad features can be calculated with the SRFT approach, while sharp features can be calculated using GSR for the power spectrum (eq. (3.29)) and the in-in approach for the bispectrum (eq. (3.45)).

Furthermore, we have carried out a statistical search for localized oscillatory features in the CMB power spectrum produced by a transient reduction in the speed of sound. We have found a number of fits and calculated the associated primordial bispectra. The bispectrum prediction resembles templates that were tested by the Planck collaboration, so we can compare our predictions with the templates used in that search. Using the 2013 data and Planck bispectrum analysis, we found a surprisingly good agreement. This is remarkable, considering that these bispectrum features are *predicted from a search in the CMB power spectrum* with a very simple ansatz for c_s. The new release made by Planck calls for a new analysis, but from their bispectrum analysis it seems that a shift in the best fit frequencies of the power spectrum will be necessary in order to find an interesting correlation.

We emphasize that the CMB power spectrum data alone can hardly justify the introduction of features on top of the ΛCDM model; a gain of $|\Delta\chi^2| \lesssim 10$ is not uncommon. However, as we have shown, low-significance fits in the power spectrum can still predict correlated features that may be observable in the CMB bispectrum. Therefore, model selection should take into account both observables simultaneously.

Our results suggest that, by exploiting correlations between different observables, current data might already be sensitive enough to detect transient reductions in the speed of sound as mild as a few percent, opening a new window for the presence of extra degrees of freedom during inflation.